AIP | The Journal of Chemical Physics

Time-dependent density functional theory excited state nonadiabatic dynamics combined with quantum mechanical/molecular mechanical approach: Photodynamics of indole in water

Matthias Wohlgemuth, Vlasta Bonačić-Koutecký, and Roland Mitrić

Citation: The Journal of Chemical Physics **135**, 054105 (2011); doi: 10.1063/1.3622563

View online: http://dx.doi.org/10.1063/1.3622563

View Table of Contents: http://scitation.aip.org/content/aip/journal/jcp/135/5?ver=pdfcov

Published by the AIP Publishing

Time-dependent density functional theory excited state nonadiabatic dynamics combined with quantum mechanical/molecular mechanical approach: Photodynamics of indole in water

Matthias Wohlgemuth,[1] Vlasta Bonačić-Koutecký,[2] and Roland Mitrić[1,a)]
[1]*Department of Physics, Freie Universität Berlin, Arnimallee 14, 14195 Berlin, Germany*
[2]*Department of Chemistry, Humboldt-Universität zu Berlin, Brook-Taylor-Str. 2, 12489 Berlin, Germany*

(Received 24 September 2010; accepted 15 July 2011; published online 3 August 2011)

We present a combination of time-dependent density functional theory with the quantum mechanical/molecular mechanical approach which can be applied to study nonadiabatic dynamical processes in molecular systems interacting with the environment. Our method is illustrated on the example of ultrafast excited state dynamics of indole in water. We compare the mechanisms of nonradiative relaxation and the electronic state lifetimes for isolated indole, indole in a sphere of classical water, and indole + $3H_2O$ embedded in a classical water sphere. In the case of isolated indole, the initial excitation to the S_2 electronic state is followed by an ultrafast internal conversion to the S_1 state with a time constant of 17 fs. The S_1 state is long living (>30 ps) and deactivates to the ground state along the N–H stretching coordinate. This deactivation mechanism remains unchanged for indole in a classical water sphere. However, the lifetimes of the S_2 and S_1 electronic states are extended. The inclusion of three explicit water molecules opens a new relaxation channel which involves the electron transfer to the solvent, leading eventually to the formation of a solvated electron. The relaxation to the ground state takes place on a time scale of 60 fs and contributes to the lowering of the fluorescence quantum yield. Our simulations demonstrate the importance of including explicit water molecules in the theoretical treatment of solvated systems. © *2011 American Institute of Physics*. [doi:10.1063/1.3622563]

I. INTRODUCTION

The excited state photoinduced dynamics of molecules is characterized by nonadiabatic processes in which the coupling between the nuclear and electronic motion leads to nonradiative transitions between electronic states. Numerous fundamental photochemical processes, such as internal conversion, electron and proton transfer, photoisomerization etc., rely fundamentally on the nonadiabatic effects.[1–5] Therefore, the accurate and efficient theoretical description of nonadiabatic processes is highly desirable. A generally applicable approach for this purpose is the mixed quantum-classical dynamics in which the nuclear motion is described by classical trajectories obtained in the framework of molecular dynamics "on the fly" combined with Tully's surface hopping (TSH) procedure.[6,7] The forces and nonadiabatic couplings required to propagate nuclear trajectories can be obtained using different *ab initio*[8–15] or semiempirical methods[16–21] for the electronic structure. In particular, the time-dependent density functional theory (TDDFT) represents an efficient generally applicable method for the description of optical properties in complex systems.[22,23] Therefore, different approaches for the nonadiabatic dynamics in the framework of TDDFT have been recently developed and successfully applied.[12–15,24] In connection with nonadiabatic processes, the ability of linear response TDDFT to describe conical intersections between excited states and the ground state has been critically examined in the literature.[15,25] The conclusion has been made that while the topology of the S_1–S_0 crossing region may not be exact, this often does not influence the relaxation pathways and photochemistry of the studied examples substantially. Moreover, a recent study of the nonadiabatic dynamics of pyrrole has demonstrated that TDDFT can provide mechanism and timescales of the nonradiative processes which are comparable to those obtained from high level correlated *ab initio* treatment.[26] Successful applications of TDDFT nonadiabatic dynamics steadily grow and have already significantly contributed towards understanding of the mechanisms of photochemical processes in complex systems[13–15,27,28] and have also been verified by comparison with experimental data.[27,29–32] In addition, the recent implementation of the first-order nonadiabatic coupling vectors in the frame of TDDFT (Refs. 33–36) has allowed to compare the nonadiabatic couplings obtained from TDDFT with those from high level correlated methods giving encouraging results on several examples. This provides the theoretical basis for the systematic investigation of the regions around conical intersections and to assess the accuracy of TDDFT in describing them.

Particularly challenging for excited state dynamics simulations is the inclusion of the environment which can have a significant influence on the course of photochemical processes.[37–39] In this context, especially the influence of solvents has drawn a particular attention of both theoretical and experimental research.[40–43] Specifically, the influence of solvents on the conical intersection dynamics has been previously extensively investigated, giving valuable insights into

a)Electronic mail: mitric@zedat.fu-berlin.de.

the mechanisms which can lead to the dramatic change of the excited state dynamics upon solvation.[44–46] The solvent effects can be treated using both continuous as well as discrete models. In the continuum models, the solute molecule is embedded in a dielectric continuum that represents the solvent.[47–51] Therefore, the specific solvent influence beyond the dielectric properties such as hydrogen bonding cannot be captured within these models. The alternative is the use of discrete models, such as quantum mechanical/molecular mechanical (QM/MM) model, where the solute molecule and perhaps a small number of solvent molecules from the closest environment are treated by electronic structure methods, while the rest of the solvent is represented by classical force field methods.[52–55] The QM/MM nonadiabatic dynamics in the framework of both semiempirical[45,56–58] as well as high level *ab initio* methods[59] has been previously introduced and successfully applied.

However, although the combination of TDDFT with QM/MM has already been established and used for the simulation of stationary optical properties of chromophores in solution[60] as well as in protein environment,[61] the extension to nonadiabatic dynamics has not been presented until now. Due to the computational efficiency and general applicability of the TDDFT method, such combination is highly desirable and would allow to push the limit of nonadiabatic dynamics simulations towards complex systems such as a variety of biochromophores in a protein environment or solvated chromophores. Of course, the well-known deficiencies of TDDFT, such as the failure to describe long range charge transfer excitations, have to be carefully examined in the context of particular applications. Therefore, in this contribution we present the combination of TDDFT nonadiabatic dynamics with the QM/MM approach and illustrate its applicability to chromophores interacting with the environment on the example of indole in water.

Indole represents a chromophore unit which is found in the amino acid tryptophan that is mainly responsible for the fluorescence of proteins.[62] Since in tryptophan as well as in indole the fluorescence quantum yield and the UV absorption are strongly dependent on the molecular environment, the fluorescence of indole is used as an important probe for determination of protein conformations and dynamics.[63–71] The fluorescence spectra of indole also exhibit unusally large Stokes shifts in polar solvents[72,73] which can be explained by the exchange of the positions of the first two excited states occurring upon solvation. A particular role in the deactivation of indole is played by the π–σ^* (S_3) state which can be characterized as a Rydberg state.[74,75] This state crosses the S_2 and S_1 states as well as the ground electronic state, thus providing the mechanism for efficient internal conversion.[76] The π–σ^* state has a high permanent dipole moment of 12.31 D which is substantially larger than those of the energetically close-lying S_2 and S_1 states.[72,77] Therefore, it is particularly sensitive to polar solvents and thus plays an important role in the photodynamics of indole in water. As demonstrated by Sobolewski and Domcke, the π–σ^* state ejects an electron in the water environment and leads to the formation of a charge-separated state.[76,78] In water solution, this mechanism is responsible for the creation of solvated electrons.[79]

While the stationary optical properties and potential energy surfaces along selected modes have been extensively investigated and understood,[74,76,78,80–85] the photodynamics of free and solvated indole, including all degrees of freedom, has not been studied so far. Therefore, here we present the simulation of ultrafast photodynamics of free indole as well as of indole interacting with a water environment. The aim of our simulations is to identify the relaxation mechanisms and to determine the time scales for the relevant processes.

The paper is structured as follows: In Sec. II, we present the combination of the TDDFT nonadiabatic dynamics with the QM/MM approach and briefly outline the procedure for calculation of quantities needed to carry out nonadiabatic dynamics simulations in the framework of the Tully's surface hopping (TSH) method. In Sec. IV, we first present the study of the photodynamics of indole in the gas phase. In the following, we investigate the influence of classical water environment on the mechanism and the time scales of relaxation processes. In order to elucidate the effect of including explicit water molecules in the QM part of the system, we also investigate the photodynamics of indole solvated with three explicit water molecules embedded into the classical water sphere. Finally, the conclusions and outlook are given.

II. THEORETICAL FORMULATION

We present first briefly the theoretical formulation of nonadiabatic dynamics in the frame of TDDFT combined with the Tully's surface hopping procedure. Subsequently, we introduce its extension in the frame of the QM/MM method.

A. TDDFT surface hopping nonadiabatic dynamics

In the frame of the surface hopping approach, the electronic wavefunction is represented in the basis of adiabatic Born-Oppenheimer states which are parametrically dependent on the classical nuclear trajectory $\mathbf{R}(t)$ according to

$$|\Psi(\mathbf{r};\mathbf{R}(t))\rangle = \sum_K C_K(t)\,|\Psi_K(\mathbf{r};\mathbf{R}(t))\rangle\,, \tag{1}$$

where $|\Psi_K(\mathbf{r};\mathbf{R}(t))\rangle$ represents the adiabatic electronic state K, while the $C_K(t)$ are the time-dependent expansion coefficients. The nuclear trajectories $\mathbf{R}(t)$ are obtained by solving the classical Newton's equations of motion. The time evolution of the electronic state coefficients $C_K(t)$ along a given classical trajectory is obtained by solving the time-dependent Schrödinger equation,

$$i\hbar\frac{dC_K(t)}{dt} = E_K C_K(t) - i\hbar\sum_I \left\langle \Psi_K(\mathbf{r};\mathbf{R}(t)) \right| \times \left| \frac{\partial \Psi_I(\mathbf{r};\mathbf{R}(t))}{\partial t} \right\rangle C_I(t), \tag{2}$$

where E_K represents the energy of the electronic state K and the second term corresponds to the nonadiabatic coupling D_{KI} between the states I and K. The latter is calculated using

the finite difference approximation according to[7]

$$D_{KI}\left(\mathbf{R}\left(t+\frac{\Delta}{2}\right)\right) \approx \frac{1}{2\Delta}(\langle\Psi_K(\mathbf{r};\mathbf{R}(t))\,|\Psi_I(\mathbf{r};\mathbf{R}(t+\Delta))\rangle - \langle\Psi_K(\mathbf{r};\mathbf{R}(t+\Delta))\,|\Psi_I(\mathbf{r};\mathbf{R}(t))\rangle), \tag{3}$$

where Δ is the time step used for the integration of the classical Newton's equations of motion.

The essential quantities needed to perform the nonadiabatic dynamics simulations are the nonadiabatic couplings D_{KI} together with the forces acting on the nuclei in the excited electronic states. In order to calculate the nonadiabatic couplings in the framework of the TDDFT method, we use an ansatz for the excited state electronic wavefunction[12,13] in terms of singly excited configurations from the manifold of occupied to virtual Kohn-Sham (KS) orbitals:

$$|\Psi_K(\mathbf{r};\mathbf{R}(t))\rangle = \sum_{i,a} c_{i,a}^K \left|\Phi_{i,a}^{CSF}(\mathbf{r};\mathbf{R}(t))\right\rangle, \tag{4}$$

where $c_{i,a}^K$ represents the CI coefficients and $|\Phi_{i,a}^{CSF}(\mathbf{r};\mathbf{R}(t))\rangle$ is a singlet spin adapted configuration state function (CSF) defined as

$$\left|\Phi_{i,a}^{CSF}(\mathbf{r};\mathbf{R}(t))\right\rangle = \frac{1}{\sqrt{2}}\left(\left|\Phi_{i\alpha}^{a\beta}(\mathbf{r};\mathbf{R}(t))\right\rangle + \left|\Phi_{i\beta}^{a\alpha}(\mathbf{r};\mathbf{R}(t))\right\rangle\right), \tag{5}$$

with $|\Phi_{i\alpha}^{a\beta}(\mathbf{r};\mathbf{R}(t))\rangle$ and $|\Phi_{i\beta}^{a\alpha}(\mathbf{r};\mathbf{R}(t))\rangle$ representing Slater determinants with single excitations from occupied orbital i to virtual orbital a with spins α or β, respectively. Although we have recently extended the TDDFT nonadiabatic dynamics also to open shell systems,[86] we present here only the closed shell formulation for simplicity.

As shown in a series of previous publications,[13,14] for nonhybrid functionals without exact exchange contribution, the CI coefficients $c_{i,a}^K$ giving rise to mutually orthogonal electronic states can be calculated from the TDDFT eigenvectors according to

$$c_{i,a}^K = (\epsilon_a - \epsilon_i)^{-1/2}\left(X_{ia}^K + Y_{ia}^K\right), \tag{6}$$

where X and Y represent the solution of the TDDFT eigenvalue problem and ϵ_a and ϵ_i are the energies of virtual and occupied molecular orbitals (MOs), respectively.

In order to calculate the nonadiabatic couplings based on the discrete approximation in Eq. (3), the overlap between two CI wavefunctions at times t and $t+\Delta$ is needed:

$$\langle\Psi_K(\mathbf{r};\mathbf{R}(t))|\Psi_I(\mathbf{r};\mathbf{R}(t+\Delta))\rangle = \sum_{ia}\sum_{i'a'} c^{*K}_{i,a} c^I_{i',a'} \left\langle\Phi_{i,a}^{CSF}(\mathbf{r};\mathbf{R}(t))\middle|\Phi_{i',a'}^{CSF}(\mathbf{r};\mathbf{R}(t+\Delta))\right\rangle. \tag{7}$$

This expression (Eq. (7)) can be reduced to the overlap of singly excited Slater determinants using Eq. (5), which can be calculated from the overlap of spatial KS orbitals. The latter ones can be further reduced to the overlap integrals involving atomic basis functions $b_k(\mathbf{R}(t))$ and $b'_m(\mathbf{R}(t+\Delta))$ and the MO coefficients $d_{ik}(t)$ and $d'_{jm}(t+\Delta)$:

$$\left\langle\phi_i(t)\left|\phi'_{j'}(t+\Delta)\right.\right\rangle = \sum_{k=1}^{n}\sum_{m=1}^{n} d_{ik}(t) d'_{jm}(t+\Delta) \times\langle b_k(\mathbf{R}(t))|b'_m(\mathbf{R}(t+\Delta))\rangle. \tag{8}$$

The two sets of basis functions $b_k(\mathbf{R}(t))$ and $b'_m(\mathbf{R}(t+\Delta))$ are centered at different positions $\mathbf{R}(t)$ and $\mathbf{R}(t+\Delta)$ and, therefore, do not form an orthonormal basis set.

From the time-dependent electronic state coefficients $C_K(t)$ which are obtained by the numerical solution of Eq. (2), using the nonadiabatic couplings described above, we calculate the hopping probabilities P_{KI} needed for switching the trajectory between the electronic states in the framework of the TSH procedure. In our approach (cf. Ref. 12), we calculate the hopping probabilities at each time step during the integration of Eq. (2) according to

$$P_{KI}(\tau) = -2\frac{\Delta\tau[Re(C_K^*(\tau)C_I(\tau)D_{KI}(\tau))]}{C_K(\tau)C_K^*(\tau)}. \tag{9}$$

The $\Delta\tau$ represents the time step used for the numerical integration of Eq. (2) for the electronic state coefficients and is typically much smaller than the nuclear time step Δ.

Since the nonadiabatic coupling D_{KI} is calculated only at the midpoint $t+\Delta/2$ between two nuclear time steps (cf. Eq. (3)), the $D_{KI}(\tau)$ needed to determine the $P_{KI}(\tau)$ according to Eq. (9) is obtained by linear interpolation in the interval $[t,t+\Delta/2]$ and extrapolation in the interval $[t+\Delta/2,t+\Delta]$. In order to eliminate possible random phase variations in the nonadiabatic coupling, the phases of the CI-like wavefunction coefficients c_{ia}^K in Eq. (4) and the KS orbital coefficients (cf. Eq. (8)) are aligned in each nuclear time step to the previous ones. After a successful hop, the conservation of energy is imposed by rescaling the nuclear velocities uniformly.

B. Combination of the TDDFT nonadiabatic dynamics with the QM/MM approach

The extension of the TDDFT nonadiabatic dynamics with the QM/MM approach is relatively straightforward. The idea is to separate the system into the quantum mechanical part (QM), for which the excited state energies, gradients, and nonadiabatic couplings are calculated in the frame of the TDDFT method, and the classical part (MM), which is treated using common force field methods. The interaction of the QM and MM regions can be accounted for using either the mechanical embedding or the electrostatic embedding scheme.[87] Since the main intention of the present work is to treat the nonadiabatic relaxation of a solute in a polar water environment, we choose the electrostatic embedding scheme. For this purpose, the QM region is electronically embedded in the MM region by including the point charges from the MM part into the one-electron Hamiltonian of the QM system. These point charges have fixed values during the simulation which are taken from the parametrization of standard force fields. In this way, the polarization of the wavefunction in the QM region by the MM point charges is taken into account. This type of QM/MM treatment is suitable for treating the excited states

of the solute under the direct influence of solvent molecules allowing to treat the inhomogeneities of solvent electric fields as well as the effect of hydrogen bonding. In the case that both the QM part (X) as well as the MM part (Y) are sufficiently well described by the classical force fields, both the effect of sterical repulsion of the QM and MM parts as well as the electrostatic interaction can be calculated as the difference between the MM energy of the combined system (X + Y) and the QM system alone. The total energy of the excited electronic state of the solute in the frame of TDDFT/MM approach can be written as

$$E_{TDDFT+MM} = E_{TDDFT}(X) + (E_{MM}(X+Y) - E_{MM}(X)) - \sum_{i,j}^{X,Y} \left(\frac{Z_i Z_j e^2}{4\varepsilon_0 \pi r_{ij}} \right). \quad (10)$$

Since in this approach the polarization of the QM system is already taken into account, the classical electrostatic interaction between the QM and MM part has to be subtracted. The forces needed to carry out dynamics "on the fly" are obtained as the derivative of Eq. (10) and the nonadiabatic couplings are calculated only for the QM part. We have implemented our approach by developing a general interface to several quantum chemical packages.[88] In particular, the TDDFT/MM approach is carried out with the TURBOMOLE package[89] or alternatively with the GAUSSIAN 09 program[90] which are used to calculate the energies and gradients of the QM part of the system. These quantities together with the TDDFT eigenvectors and MO coefficients are read by the interface program and used to compute the nonadiabatic couplings and to carry out the surface hopping procedure. The MM part of the system is treated using the TINKER package[91] and the gradients are also fed into the interface. In addition to the TDDFT approach, the approximate tight-binding version (TDDFTB (Ref. 43)) can be also employed within our TDDFT/MM approach.

III. COMPUTATIONAL DETAILS

The geometry of isolated indole has been optimized using the DFT method with Perdew-Burke-Ernzerhof (PBE) functional[92,93] and the triple-zeta valence plus polarization (TZVP) basis set.[94] The initial conditions for the nonadiabatic dynamics have been obtained from a 30 ps DFT trajectory at $T = 300$ K by sampling at regular time intervals. In total 120 initial conditions have been generated.

The model for the solvated indole has been obtained by embedding indole in a 50 Å cubic water box and equilibrating using force field molecular dynamics under periodic boundary conditions over 200 ps at p= 1.0 bar and $T = 300$ K. For indole, the OPLS-AA (Refs. 95–99) force field and for water the TIP-3P (Ref. 100) force field were used. After equilibration, a 24 Å radius sphere, including indole and 1944 water molecules, was cut from the box and further relaxed using the DFT/MM method with the PBE functional[92,93] for 25 ps at $T = 300$ K. For the atoms in the QM part, the TZVP basis set[94] was used and the MM part of the system was described using the same force fields as for the equilibration. The initial conditions for the nonadiabatic dynamics simulations were generated by sampling the DFT/MM trajectory at regular time intervals. Totally, 100 initial conditions have been generated for starting the nonadiabatic dynamics simulations. The water spheres of each structure in the initial ensemble were further truncated to 20 Å in order to obtain an almost spherical water droplet.

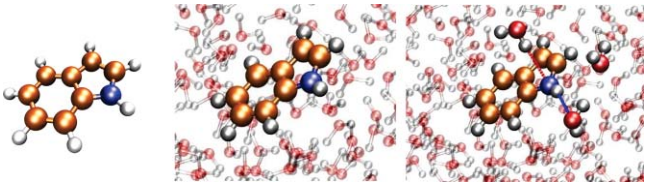

FIG. 1. DFT and DFT/MM optimized structures of indole (left), indole in a classical water sphere (middle), and indole + $3H_2O$ (right) in a classical water sphere, respectively.

The nonadiabatic dynamics simulations have been performed for three systems: (i) isolated indole (Fig. 1, left), (ii) indole as QM part embedded in a MM water sphere (Fig. 1, middle), and (iii) indole + $3H_2O$ as a QM part embedded in a MM water sphere (Fig. 1, right). The systems have been chosen in order to examine both the influence of the classical environment as well as the inclusion of explicit water molecules on the nonadiabatic dynamics. The water molecules in system (iii) have been selected according to a proximity criterion with respect to the N–H bond. This allows us to investigate also the influence of the hydrogen bonding of water with the N–H hydrogen atom, as well as the nitrogen of indole.

The nonadiabatic dynamics has been performed in the framework of our TDDFT/MM approach using the PBE functional[92,93] for the QM part combined with TZVP basis set[94] and the same force fields as for the equilibration. Additionally, in order to speed up the MD simulations, the resolution of the identity (RI) approximation[101,102] has been employed for the TDDFT calculations. For the integration of the nuclear equations of motion, the velocity Verlet algorithm[103] has been used with a time step of 0.1 fs. The electronic Schrödinger equation (Eq. (2)) has been integrated using the fourth order Runge-Kutta method with a time step of 10^{-5} fs. We have propagated trajectories in a manifold of the ground and seven electronic excited states for all three systems.

In order to validate the accuracy of our results, we have calculated the absorption spectra of isolated and solvated indole using the CC2 method[104] as implemented in the TURBOMOLE package[89] as well as using the Coulomb attenuated B3LYP (CAM-B3LYP) density functional,[105] which has been developed in order to improve the description of long-range charge transfer transitions and is implemented in the GAUSSIAN 09 program suite.[90] In addition, our implementation of TDDFT/MM nonadiabatic dynamics has been extended to the CAM-B3LYP functional and a small number of trajectories has been propagated using this method. However, since the nonadiabatic dynamics with the CAM-B3LYP functional is computationally considerably more expensive than with the PBE functional, only a limited number of trajectories could be propagated within reasonable computational time.

IV. RESULTS AND DISCUSSION

We present first the results of the nonadiabatic photodynamics for isolated indole, then for indole in a classical sphere of water, and finally for indole interacting with three explicit water molecules in the QM part and embedded in a large classical sphere of water. The purpose of this comparison is to reveal the effect of the environment and the importance of explicit quantum mechanical treatment of selected water molecules.

A. Isolated indole

TDDFT with RI-PBE/TZVP gives rise to two energetically close π–π^* transitions at 4.38 eV (S_1) and 4.60 eV (S_2) with relatively low oscillator strengths which compares well with the experimental values of 4.4 eV (S_1) and 4.8 eV (S_2).[106] The dark S_3 state with π–σ^* character is located at 5.3 eV in our TDDFT calculations which is comparable to the previous CASPT2 value of Sobolewski and Domcke of 5.05 eV.[78] The first two excited states can be characterized according to the Platt nomenclature as L_a and L_b. The L_a state is characterized by a high permanent dipole moment and has a charge transfer character, while the L_b state has a low permanent dipole moment and is a locally excited state. The energetic position of these two states and its dependence on the polarity of solvents has been intensively studied both theoretically and experimentally.[75,77,107–109] As reported previously, the L_b state is the lowest state in the gas phase as well as in nonpolar solvents, while the L_a state is the lowest state in polar solvents. This is due to the higher permanent dipole moment of the L_a state which renders it more sensitive to the polar environment. In our TDDFT calculations using the PBE functional as presented in Fig. 2(a), the lowest energy transition mainly involves a HOMO → LUMO excitation and has a larger dipole moment than the S_2 state which has a main contribution from HOMO → LUMO + 1

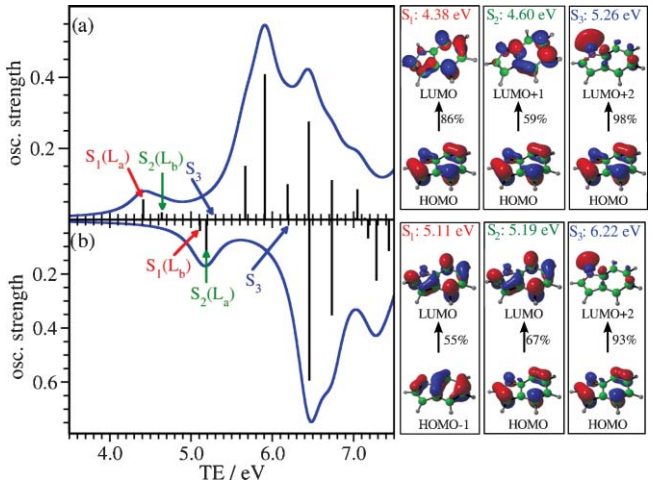

FIG. 2. Absorption spectrum of isolated indole calculated using TDDFT methods (left panel) with (a) PBE functional and (b) CAM-B3LYP functional. Leading excitations contributing to the first three excited states (right panels). The calculated discrete absorption lines were convoluted with a Lorentzian width of 0.4 eV.

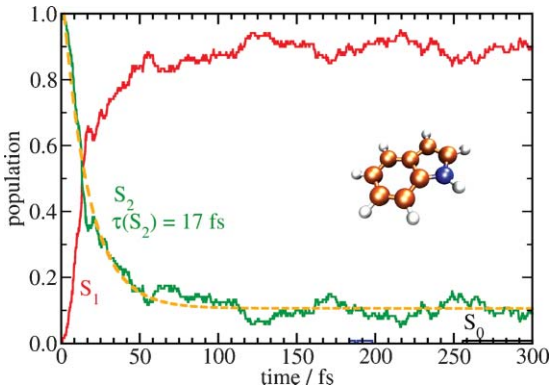

FIG. 3. Population of the ground and excited electronic states during the nonadiabatic dynamics of isolated indole. The black, red, and green curves represent the population of the S_0, S_1, and S_2 states, respectively. The dashed line represents an exponential fit for the depopulation of the S_2 state with a time constant $\tau(S_2)$ of 17 fs.

excitation and exhibits a lower dipole moment. Thus, the PBE functional does not provide the correct ordering of the L_a and L_b states. The inability of TDDFT to provide the correct ordering has been previously explained by the single reference character of TDDFT.[110] The dark π–σ^* state is located at 5.26 eV and is dominated by the HOMO → LUMO + 2 excitation, where LUMO + 2 is a σ^* orbital of the N–H bond. For comparison, the spectrum has also been calculated using the CAM-B3LYP functional. As shown in Fig. 2(b), the CAM-B3LYP excitation energy is shifted to higher values by ∼0.6 eV with respect to the experiment and the PBE calculations while the ordering of states can be assigned to $L_b(S_1)$ and $L_a(S_2)$. Sobolewski and Domcke has shown previously that the position of the π–σ^* state is very sensitive to the augmentation of the basis set and can be shifted below 5.0 eV, if, e.g., aug-ccVTZ basis set is used.[111] Notice that although the assignment of states with the PBE method is not unambiguous, in a thermal ensemble these two states will largely overlap since their energy difference is very small.

In order to study the excited state photodynamics, we have launched 120 trajectories starting from the S_2 excited state and propagated them in a manifold of the ground and seven excited electronic states. The average population of the electronic states presented in Fig. 3 shows that the S_2 state is depopulated with a time constant of 17 fs, while the complete population transfer to the S_1 state occurs already after 100 fs. The S_1 state only slowly decays to the ground state, so that after 300 fs only 1% of the trajectories have returned to the ground state. This allows to conclude that the transfer to the ground state occurs mainly from the S_1 state and the lifetime of this state can be estimated to be at least 30 ps or longer. Our findings are consistent with the experiments on the gas phase indole by Lippert *et al.*[109] who have found that for the indole molecule efficient coupling between the π–π^* and π–σ^* states does not exist, leading to a stable excited state population over a time of 100 ps. As shown on the example of one selected trajectory in Fig. 4(a), the mechanism of the relaxation to the ground electronic state involves the excitation of the N–H bond stretching which takes place after the π–π^* to π–σ^* nonadiabatic transition, in this example occurring after 180 fs. In Fig. 4(b), the N–H bond distance is shown

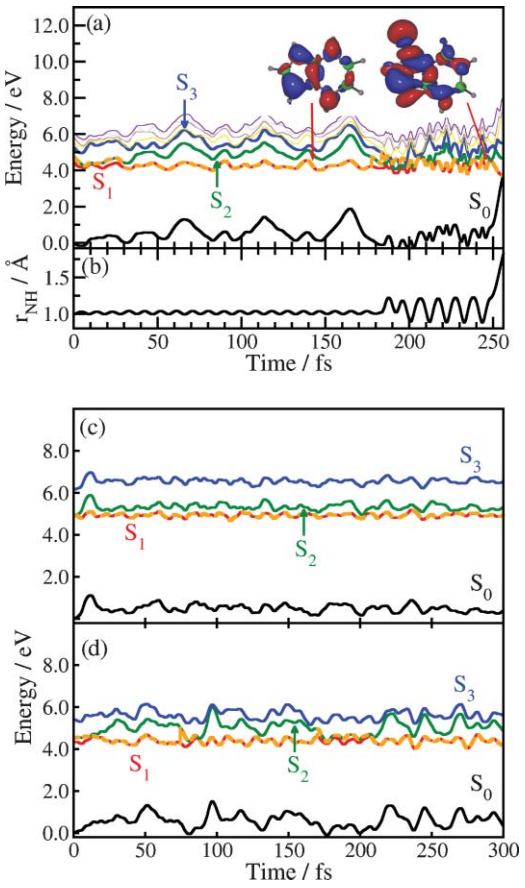

FIG. 4. (a) Energies of the electronic states along a selected nonadiabatic trajectory of isolated indole which relaxes to electronic ground state using PBE functional. The insets show the electron density difference of the electronic excited state and the ground state at 140 fs (π–π^*) and 250 fs (π–σ^*), respectively. (b) N–H bond length along the trajectory. (c) Energies of the electronic states along a selected nonadiabatic trajectory of isolated indole using CAM-B3LYP functional. (d) Energies of the electronic states along a selected nonadiabatic trajectory of isolated indole using PBE functional. The actual state in which the trajectory resides is labeled by the orange dashed line.

as a function of time, clearly illustrating strong excitation of the N–H stretching vibration. The return to the ground electronic state occurs at 255 fs. The relaxation mechanism involving the N–H bond stretching has been predicted by Sobolowski and Domcke[74,76] and was confirmed experimentally.[112,113] The experiments of Nix *et al.* have shown that the dissociation of indole in the π–σ^* state constitutes a small fraction of the total H atom yield, while most of the observed atoms are attributable to the multiphoton absorption.[112,113] Since in our simulation multiphoton absorption is not included, we observe only direct dissociation on the π–σ^* state with relatively low yield.

However, as shown in Fig. 3, the major part of the population resides in the excited electronic state. For comparison, a nonadiabatic dynamics trajectory which remains in the first excited S_1 state using CAM-B3LYP functional and PBE functional is shown in Figs. 4(c) and Fig. 4(d), respectively. In both cases, the relaxation of the S_2 excited state occurs within the first 10 fs. Notice that the larger energy gap between S_2 and S_3 excited states with CAM-B3LYP functional

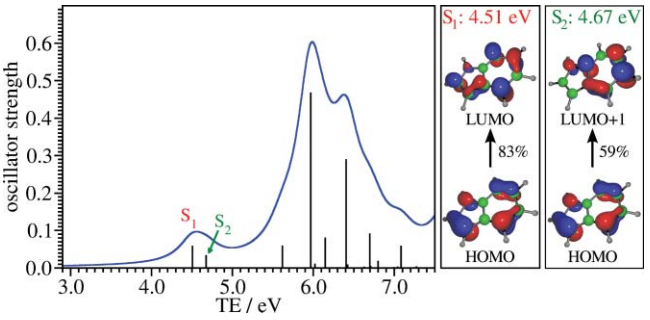

FIG. 5. Absorption spectrum of indole solvated with a classical sphere of 1993 water molecules calculated with the TDDFT/MM method (left panel). Leading excitations contributing to the first two excited states (right panel). The calculated discrete absorption lines were convoluted with a Lorentzian width of 0.4 eV.

(compared to PBE) leads to a less effective coupling of the π–π^* and π–σ^* electronic excited states and a relaxation to the π–σ^* state involving the N–H bond stretch is improbable.

B. Indole in a classical water sphere

The absorption spectrum of indole in a classical water environment is shown in Fig. 5. As can be seen, both the energetic positions as well as the intensities of the S_1 and S_2 states are almost unaffected by a classical water environment. Also, the character of the lowest electronic states remains the same as in the gas phase (cf. Fig. 2).

In order to investigate the influence of the classical water environment on the dynamical properties and the relaxation, we have run nonadiabatic dynamics, including seven excited states, using our TDDFT/MM approach. A total number of 70 trajectories has been propagated starting in the S_2 electronic state. The relative population of electronic states presented in Fig. 6 shows that the relaxation to the S_1 state occurs significantly slower than in the gas phase. The analysis of the nonadiabatic trajectories shows that the average nonadiabatic coupling between S_1 and S_2 state is systematically smaller in water than in the gas phase. This effect can be attributed to two factors: (i) polarization, which modifies the electronic wavefunctions and thus the couplings and (ii) friction, which due to the interaction of indole with water leads to slower nuclear motion in water environment and, thus, to lower values of the couplings. In contrast to isolated indole, no transition to the ground state was observed. This demonstrates the large effect that solvation can have on the rate of nonradiative processes, even if electronic effects are only approximately treated using the electrostatic embedding scheme.

C. Indole + $3H_2O$ in a classical water sphere

Finally, in order to examine the influence of including explicit water molecules in the QM part of the system, we consider indole solvated with three water molecules and embedded in a classical water sphere.

The three water molecules which were explicitly included in the simulation were selected according to a proximity criterion with respect to the N–H group of the indole ring. Specifically, the three water molecules closest to the H-atom

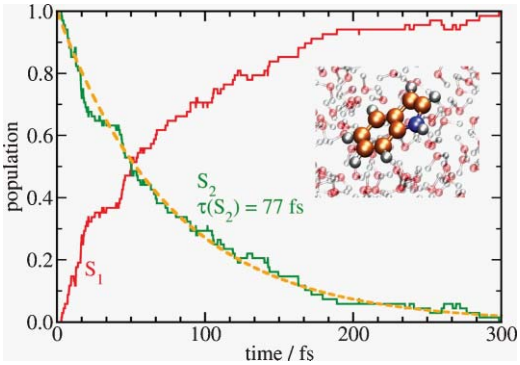

FIG. 6. Population of the excited electronic states during the nonadiabatic dynamics of indole in a classical water sphere. The red and green curves represent the population of the S_1 and S_2 states, respectively. The orange dashed line represents an exponential fit for the depopulation of the S_2 state with a time constant $\tau(S_2)$ of 77 fs.

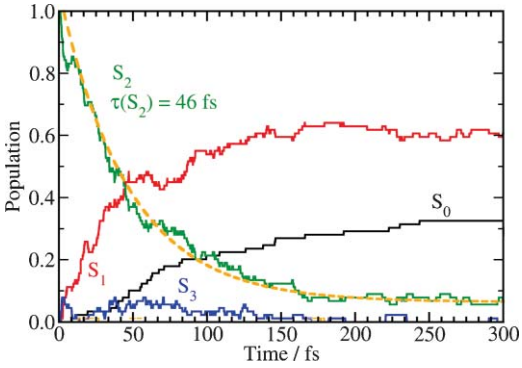

FIG. 8. Population of the ground and excited electronic states during the nonadiabatic dynamics of indole and $3H_2O$ in a classical water sphere. The black, red, and green curves represent the population of the S_0, S_1, and S_2 states, respectively. The orange dashed line represents an exponential fit for the population of the S_2 state with a time constant $\tau(S_2)$ of 46 fs.

of the N–H group have been selected. This results in a model in which one water molecule forms a hydrogen bond with the N-atom, one is hydrogen bonded to the H-atom of the N–H group, and an additional water molecule is bound to the second one (cf. Fig. 1 right). Due to the fact that the main relaxation coordinate of indole in the gas phase involves the N–H bond stretching, it is plausible to assume that water surrounding the N–H bond will most strongly influence the dynamics.

The absorption spectrum of solvated indole using the TDDFT/MM approach is shown in Fig. 7(a). Again, the solvation does not strongly influence the position of the electronic states but there is a small redistribution of the intensities. The S_1 and S_2 states are, in our TDDFT calculations, located at 4.34 and 4.57 eV, which almost perfectly agrees with the experimental values of 4.31 eV and 4.59 eV (cf. Ref. 78, and the references therein). The electronic character of the first two excited states is analogous as in the gas phase or in a classical water sphere. However, due to the possibility of a charge transfer to the solvent molecules (CTTS)

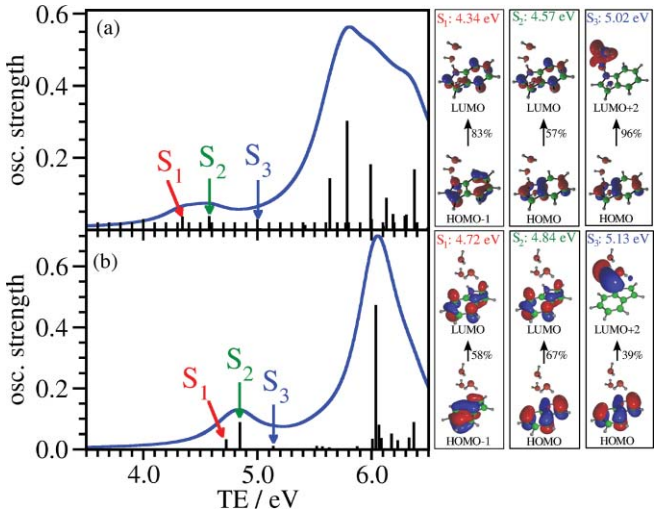

FIG. 7. Absorption spectrum of indole solvated with three explicit H_2O in a classical sphere of 1993 water molecules calculated with (a) the TDDFT/MM method and (b) CC2/aug-ccVDP method. Leading excitations contributing to the first three excited states (right panels). The calculated discrete absorption lines were convoluted with a Lorentzian width of 0.4 eV.

which are explicitly included in the QM part of the system, electronic states with new features arise and the S_3 state is now a CTTS state located at 5.02 eV. The formation of such CTTS state has been predicted by Sobolewski and Domcke in the studies of indole-water clusters.[78] The CTTS nature of the S_3 state together with the characters of the S_1 and S_2 states is demonstrated on the right side of Fig. 7(a). The shift of the S_3 state to lower energy has been confirmed also by carrying out CC2/aug-ccVDZ calculations, since it is known that TDDFT can strongly underestimate the position of long range charge transfer excited states. It should be pointed out that, as shown by Lange and Herbert,[114] this deficiency of TDDFT can be partly remedied by electrostatic embedding which is the case in our TDDFT/MM approach. For comparison, the CC2 absorption spectrum is shown in Fig. 7(b). One finds the S_1, S_2, and S_3 states shifted to 4.72 eV, 4.84 eV, and 5.13 eV compared to the TDDFT/MM spectrum. However, the S_3 state still has a CTTS character and thus confirms our findings at the TDDFT/MM level.

In our nonadiabatic dynamics simulations, we start from the second excited state and propagate 100 trajectories in the manifold of the ground and 7 excited electronic states. As shown in Fig. 8, the population transfer from the second excited state takes place with a time constant of 46 fs leading to a transient population of the S_1 state. At the end of the simulation, 32% of the trajectories have returned to the ground state. A major part of the population remains in the S_1 state and can be responsible for the fluorescence.

In contrast to the dynamics in the gas phase or in the classical water environment, the nonadiabatic dynamics with explicit consideration of water molecules leads to a deactivation to the ground state due to the formation of the CTTS state. In Fig. 9, the energies of electronic states for one selected trajectory are presented, exhibiting an electron transfer event at 45 fs. The formation of the CTTS state has been confirmed by carrying out CC2 calculations for selected structures along the TDDFT nonadiabatic trajectories. In the lower panel of Fig. 9, the molecular orbitals to which the excitation dominantly occurs are depicted for three selected time steps, demonstrating that both in TDDFT as well as in the CC2 method the CTTS state is present at 45 fs. Moreover,

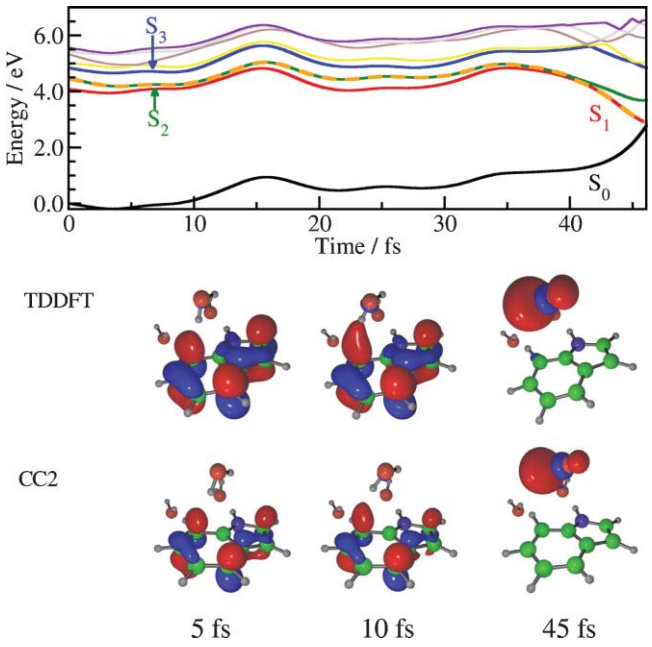

FIG. 9. (Upper part) Energies of the electronic states along a selected nonadiabatic trajectory of indole + $3H_2O$ in a classical water sphere. The actual state in which the trajectory resides is labeled by the orange dashed line. (Lower part) Molecular orbitals to which the excitation dominantly occurs along the nonadiabatic trajectory obtained using the TDDFT and CC2 methods at selected time steps. The main contribution to the excited state populated at 5 fs and 10 fs corresponds to the (π–π^*) transition in both methods, while at 45 fs, both methods give rise to the CTTS transition.

the CTTS character of the excited state is also illustrated by the electron density difference between the states in which the trajectory resides and the ground state at several time steps before and after the electron transfer occurs, as shown in Fig. 10. Such ultrafast electron transfer is ultimately responsible for the formation of solvated electrons which has also been observed experimentally.[79,115] In order to assess the importance of the electron transfer to water, we have also performed CAM-B3LYP nonadiabatic dynamics simulation for one single trajectory. The excited state energies along a typical trajectory propagated using PBE and CAM-B3LYP methods and the Kohn-Sham orbitals to which the excitation dominantly occurs at the initial geometry for three lowest excited states are shown in Fig. 11. Overall, the behavior of the S_1 and S_2 excited states in both methods is very similar.

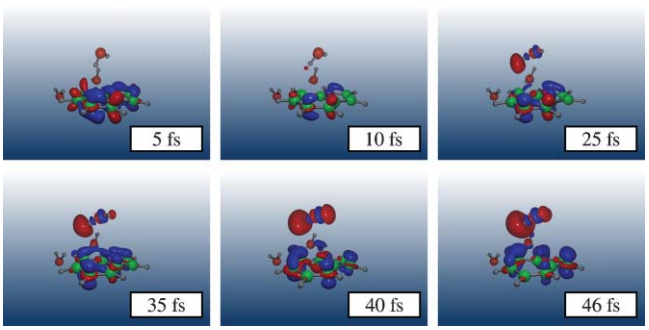

FIG. 10. Snapshots with electron density difference of the nonadiabatic dynamics simulation of indole + $3H_2O$ in a classical water sphere showing the charge transfer state to solvent.

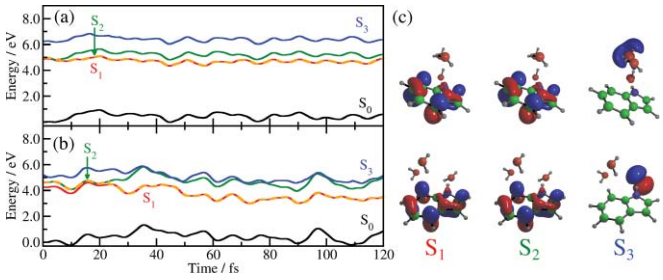

FIG. 11. Energies of the electronic states along two selected nonadiabatic trajectories of indole + $3H_2O$ in a classical water sphere using (a) CAM-B3LYP functional and (b) PBE functional. The actual state in which the trajectory resides is labeled by the orange dashed line. (c) Unoccupied molecular orbitals to which the excitation dominantly occurs at t= 0.0 fs with CAM-B3LYP (upper part) and PBE (lower part). The S_1 and S_2 states are with both functionals of π–π^* character while the S_3 has the π–σ^* character.

However, the third excited state exhibiting the electron transfer to water is about 0.6 eV lower in energy in the PBE functional than in the CAM-B3LYP (blue line in Fig. 11). This leads to stronger mixing between the S_2 and S_3 states in the simulations using the PBE functional and may cause overestimation of the importance of the electron transfer to water. However, although the electron transfer may be overestimated in the PBE method, it has been experimentally observed[79,115] and, thus, represents an important relaxation channel. To a small extent (less than 10% of the trajectories), we also observe the excited state proton transfer from indole to close water molecules occurring due to the dissociation of the N–H bond. This finding is in a good agreement with the experimental results[115] in which photoionization (formation of the CTTS state) takes place within 100 fs, without recombination over a period of several nanoseconds. In the experimental results,[115] the transition to the ground state is completed within 350 fs. The experimental quantum yield of the CTTS process was estimated to 38%, which is in very good agreement with our results. Our results show that explicit consideration of water molecules in the QM subsystem opens additional photochemical channels which could not be revealed considering only classical water environment.

V. CONCLUSION

We have presented the combination of the TDDFT excited state nonadiabatic dynamics with the QM/MM approach which is generally applicable to the simulation of ultrafast photodynamics of systems interacting with the environment. We have illustrated our approach by studying the influence of water on the photodynamics of (i) isolated indole in the gas phase, (ii) indole interacting only with a classical water sphere, as well as (iii) indole interacting with three explicit water molecules embedded in water. We have shown that, in general, a classical water environment leads to an extension of the electronic state lifetimes of indole. In particular, for indole in a classical water sphere, the relaxation mechanism is analogous to the one in the gas phase and involves an ultrafast $S_2 \rightarrow S_1$ transition. The inclusion of explicit water molecules opens a new relaxation channel which involves the electron transfer to water, leading eventually to the creation of solvated electrons. This channel competes with

the relaxation mechanism present in isolated indole. Our simulations demonstrate that the explicit consideration of water molecules close to the chromophore may be important since it can open new photochemical channels which would not be present, if all solvent molecules were treated classically. Our approach will, in the future, be extended to studies of the photodynamics of chromophores in proteins, on surfaces or interacting with different nanostructures.

ACKNOWLEDGMENTS

M.W. and R.M. gratefully acknowledge the Deutsche Forschungsgemeinschaft (DFG) for the financial support within the Emmy-Noether program (ENP-MI-1236).

[1] J. Michl and V. Bonačić-Koutecký, *Electronic Aspects of Organic Photochemistry* (Wiley, New York, 1990).
[2] *Conical Intersections*, Advanced Series in Physical Chemistry Vol. 15, edited by W. Domcke, D. R. Yarkony, and H. Köppel (World Scientific, Singapore, 2004).
[3] M. A. Robb, M. Garavelli, M. Olivucci, and F. Bernardi, Rev. Comput. Chem. **15**, 87 (2000).
[4] A. H. Zewail, J. Phys. Chem. A **104**, 5660 (2000).
[5] M. Bixon and J. Jortner, J. Chem. Phys. **48**, 715 (1968).
[6] J. C. Tully, J. Chem. Phys. **93**, 1061 (1990).
[7] S. Hammes-Schiffer and J. C. Tully, J. Chem. Phys. **101**, 4657 (1994).
[8] H. Lischka, M. Dallos, P. G. Szalay, D. R. Yarkony, and R. Shepard, J. Chem. Phys. **120**, 7322 (2004).
[9] H. Lischka, M. Dallos, and R. Shepard, Mol. Phys. **100**, 1647 (2002).
[10] R. Mitrić, V. Bonačić-Koutecký, J. Pittner, and H. Lischka, J. Chem. Phys. **125**, 024303 (2006).
[11] N. L. Doltsinis and D. Marx, Phys. Rev. Lett. **88**, 166402 (2002).
[12] E. Tapavicza, I. Tavernelli, and U. Rothlisberger, Phys. Rev. Lett. **98**, 023001 (2007).
[13] U. Werner, R. Mitrić, T. Suzuki, and V. Bonačić-Koutecký, Chem. Phys. **349**, 319 (2008).
[14] R. Mitrić, U. Werner, and V. Bonačić-Koutecký, J. Chem. Phys. **129**, 164118 (2008).
[15] E. Tapavicza, I. Tavernelli, U. Rothlisberger, C. Filippi, and M. E. Casida, J. Chem. Phys. **129**, 124108 (2008).
[16] G. Granucci, M. Persico, and A. Toniolo, J. Chem. Phys. **114**, 10608 (2001).
[17] A. Koslowski, M. E. Beck, and W. Thiel, J. Comput. Chem. **24**, 714 (2003).
[18] S. Patchkovskii, A. Koslowski, and W. Thiel, Theor. Chem. Acc. **114**, 84 (2005).
[19] E. Fabiano and W. Thiel, J. Phys. Chem. A **112**, 6859 (2008).
[20] E. Fabiano, T. W. Keal, and W. Thiel, Chem. Phys. **349**, 334 (2008).
[21] Z. Lan, E. Fabiano, and W. Thiel, J. Phys. Chem. B **113**, 3548 (2009).
[22] A. Dreuw and M. Head-Gordon, Chem. Rev. **105**, 4009 (2005).
[23] M. E. Casida, J. Mol. Struct.: THEOCHEM **914**, 3 (2009).
[24] C. F. Craig, R. W. Duncan, and O. V. Prezhdo, Phys. Rev. Lett. **95**, 163001 (2005).
[25] B. G. Levine, C. Ko, J. Quenneville, and T. J. Martinez, Mol. Phys. **104**, 1039 (2006).
[26] M. Barbatti, J. Pittner, M. Pederzoli, U. Werner, R. Mitrić, V. Bonačić-Koutecký, and H. Lischka, Chem. Phys. **375**, 26 (2010).
[27] U. Werner, R. Mitrić, and V. Bonačić-Koutecký, J. Chem. Phys. **132**, 174301 (2010).
[28] O. V. Prezhdo, Acc. Chem. Res. **42**, 2005 (2009).
[29] Y.-I. Suzuki, T. Fuji, T. Horio, and T. Suzuki, J. Chem. Phys. **132**, 174302 (2010).
[30] T. Fuji, Y.-I. Suzuki, T. Horio, T. Suzuki, R. Mitrić, U. Werner, and V. Bonačić-Koutecký, J. Chem. Phys. **133**, 234303 (2010).
[31] A. Kumar, M. Kolaski, and S. Kim, J. Chem. Phys. **128**, 034304 (2008).
[32] I. Frank and K. Damianos, Chem. Phys. **343**, 347 (2008).
[33] I. Tavernelli, E. Tapavicza, and U. Rothlisberger, J. Chem. Phys. **130**, 124107 (2009).
[34] I. Tavernelli, B. F. E. Curchod, and U. Rothlisberger, J. Chem. Phys. **131**, 196101 (2009).
[35] I. Tavernelli, B. F. E. Curchod, A. Laktionov, and U. Rothlisberger, J. Chem. Phys. **133**, 194104 (2010).
[36] R. Send and F. Furche, J. Chem. Phys. **132**, 044107 (2010).
[37] C. E. Crespo-Hernández, B. Cohen, P. M. Hare, and B. Kohler, Chem. Rev. **104**, 1977 (2004).
[38] M. Glasbeek and H. Zhang, Chem. Rev. **104**, 1929 (2004).
[39] I. Burghardt and J. T. Hynes, J. Phys. Chem. A **110**, 11411 (2006).
[40] J.-M. L. Pecourt, J. Peon, and B. Kohler, J. Am. Chem. Soc. **123**, 10370 (2001).
[41] R. Improta and V. Barone, J. Am. Chem. Soc. **126**, 14320 (2004).
[42] T. Gustavsson, A. Banyasz, E. Lazzarotto, D. Markovitsi, G. Scalmani, M. Frisch, V. Barone, and R. Improta, J. Am. Chem. Soc. **128**, 607 (2006).
[43] R. Mitrić, U. Werner, M. Wohlgemuth, G. Seifert, and V. Bonačić-Koutecký, J. Phys. Chem. A **113**, 12700 (2009).
[44] A. Toniolo, G. Granucci, and T. J. Martinez, J. Phys. Chem. A **107**, 3822 (2003).
[45] A. Toniolo, C. Ciminelli, G. Granucci, T. Laino, and M. Persico, Theor. Chem. Acc. **111**, 270 (2004).
[46] T. J. Martinez, Acc. Chem. Res. **39**, 119 (2006).
[47] C. J. Cramer and D. G. Truhlar, Chem. Rev. **99**, 2161 (1999).
[48] J. Tomasi, B. Mennucci, and R. Cammi, Chem. Rev. **105**, 2999 (1999).
[49] J. Tomasi and M. Persico, Chem. Rev. **105**, 2027 (1994).
[50] J. Tomasi, Theor. Chem. Acc. **112**, 184 (2004).
[51] A. Klamt, V. Jonas, T. Bürger, and J. C.W. Lohrenz, J. Phys. Chem. A **102**, 5074 (1998).
[52] A. Warshel and M. Levitt, J. Mol. Biol. **103**, 227 (1976).
[53] M. J. Field, P. A. Bash, and M. Karplus, J. Comput. Chem. **11**, 700 (1990).
[54] J. Gao, in *Reviews in Computational Chemistry*, edited by K. B. Lipkowski and D. B. Boyd (Wiley, New York, 1995), Vol. 7, p. 119.
[55] H. M. Senn and W. Thiel, in *Atomistic Approaches in Modern Biology*, Topics in Current Chemistry, edited by M. Reiher (Springer-Verlag, Berlin/Heidelberg, 2007), Vol. 268, pp. 173–290.
[56] M. Persico, G. Granucci, S. Inglese, T. Laino, and A. Toniolo, J. Mol. Struct.: THEOCHEM **621**, 119 (2003).
[57] S. Inglese, G. Granucci, T. Laino, and M. Persico, J. Phys. Chem. B **109**, 7941 (2005).
[58] C. Ciminelli, G. Granucci, and M. Persico, Chem. Phys. **349**, 325 (2008).
[59] M. Ruckenbauer, M. Barbatti, T. Mueller, and H. Lischka, J. Chem. Phys. A **114**, 6757 (2010).
[60] M. Parac, M. Doerr, C. M. Marian, and W. Thiel, J. Comput. Chem. **31**, 90 (2010).
[61] E. Sanchez-Garcia, M. Doerr, and W. Thiel, J. Comput. Chem. **31**, 1603 (2010).
[62] J. R. Lakowicz, *Principles of Fluorescence Spectroscopy* (Kluwer Academic/Plenum, New York, 1999).
[63] J. M. Beechem and L. Brand, Annu. Rev. Biochem. **54**, 43 (1985).
[64] Y. Chen and M. D. Barkley, Biochemistry **37**, 9976 (1998).
[65] S. V. Konev, *Fluorescence and Phosphorescence of Proteins and Nucleic Acids* (Plenum, New York, 1967).
[66] J. W. Longworth, *Excited States of Proteins and Nucleic Acids* (Plenum, New York, 1971).
[67] A. P. Demchenko, *Ultraviolet Spectroscopy of Proteins* (Springer-Verlag, New York, 1986).
[68] P. R. Callis, Methods Enzymol. **278**, 113 (1997).
[69] S. Schenkl, F. van Mourik, G. van der Zwan, S. Haacke, and M. Chergui, Science **309**, 917 (2005).
[70] M. Rodríguez, A. Lindinger, J. L. P. Lustres, S. A. Kovalenko, N. P. Ernsting, L. Wöste, and G. Sieger, Biochem. Biophys. Res. Commun. **345**, 886 (2006).
[71] M. Rodríguez, A. Lindinger, N. P. Ernsting, M. Malmsten, and G. Sieger, Arch. Biochem. Biophys. **460**, 92 (2007).
[72] I. Tatischeff, R. Klein, T. Zemb, and M. Duquesne, Chem. Phys. Lett. **54**, 394 (1978).
[73] H. Lami and N. Glasser, J. Chem. Phys. **84**, 597 (1986).
[74] A. L. Sobolewski and W. Domcke, Chem. Phys. Lett. **315**, 293 (1999).
[75] B. C. Dian, A. Longarte, and T. S. Zwier, J. Chem. Phys. **118**, 2696 (2003).
[76] A. L. Sobolewski, W. Domcke, C. Dedonder-Lardeux, and C. Jouvet, Phys. Chem. Chem. Phys. **4**, 1093 (2002).
[77] L. Serrano-Andres and B. O. Roos, J. Am. Chem. Soc. **118**, 185 (1996).
[78] A. L. Sobolewski and W. Domcke, Chem. Phys. Lett. **329**, 130 (2000).
[79] J. Peon, G. C. Hess, J.-M. L. Pecourt, T. Yuzawa, and B. Kohler, J. Chem. Phys. **103**, 2460 (1999).

[80]J. Hager and S. C. Wallace, J. Phys. Chem. **88**, 5513 (1984).
[81]R. M. Helm, M. Clara, T. L. Grebner, and H. J. Neusser, J. Phys. Chem. A **102**, 3268 (1998).
[82]T. M. Korter, D. W. Pratt, and J. Kupper, J. Phys. Chem. A **102**, 7211 (1998).
[83]M. Mons, I. Dimicoli, B. Tardivel, F. Piuzzi, V. Brenner, and P. Millie, J. Phys. Chem. A **103**, 9958 (1999).
[84]J. R. Carney and T. S. Zwier, J. Phys. Chem. A **103**, 9943 (1999).
[85]C. Dedonder-Lardeux, C. Jouvet, S. Perun, and A. Sobolewski, Phys. Chem. Chem. Phys. **5**, 5118 (2003).
[86]R. Mitrić, J. Petersen, M. Wohlgemuth, U. Werner, V. Bonačić-Koutecký, L. Wöste, and J. Jortner, J. Phys. Chem. A **115**, 3755 (2011).
[87]D. Bakowies and W. Thiel, J. Phys. Chem. **100**, 10580 (1996).
[88]The interface program is available upon request (2010).
[89]R. Ahlrichs, M. Bär, M. Häser, H. Horn, and C. Kölmel, Chem. Phys. Lett. **162**, 165 (1989).
[90]M. J. Frisch, G. W. Trucks, H. B. Schlegel *et al*., GAUSSIAN 09, Revision A.1, Gaussian, Inc., Wallingford, CT, 2009.
[91]J. W. Ponder and F. M. Richards, J. Comput. Chem. **8**, 1061 (1987).
[92]J. Perdew and Y. Wang, Phys. Rev. B **45**, 13244 (1992).
[93]J. Perdew, K. Burke, and M. Ernzerhof, Phys. Rev. Lett. **77**, 3865 (1996).
[94]K. Eichkorn, O. Treutler, H. Öhm, M. Häuser, and R. Ahlrichs, Chem. Phys. Lett. **240**, 283 (1995).
[95]W. L. Jorgensen, D. S. Maxwell, and J. Tirado-Rives, J. Am. Chem. Soc. **117**, 11225 (1996).
[96]W. L. Jorgensen and N. A. McDonald, J. Mol. Struct.: THEOCHEM **424**, 145 (1998).
[97]W. L. Jorgensen, J. P. Ulmschneider, and J. Tirado-Rives, J. Phys. Chem. B **108**, 16264 (2004).
[98]N. A. McDonald and W. L. Jorgensen, J. Phys. Chem. B **102**, 8049 (1098).
[99]R. C. Rizzo and W. L. Jorgensen, J. Am. Chem. Soc. **121**, 4827 (1999).
[100]W. L. Jorgensen, J. Chandrasekhar, J. D. Madura, R. W. Impey, and M. L. Klein, J. Chem. Phys. **79**, 926 (1983).
[101]B. I. Dunlap, J. W. D. Connolly, and J. R. Sabin, J. Chem. Phys. **71**, 3396 (1978).
[102]K. Eichhorn, O. Treuter, H. Öhm, M. Häser, and R. Ahlrichs, Chem. Phys. Lett. **109**, 40 (1995).
[103]W. C. Swope, H. C. Andersen, P. H. Berens, and K. R. Wilson, J. Chem. Phys. **76**, 637 (1982).
[104]O. Christiansen, H. Koch, and P. Jorgensen, Chem. Phys. Lett. **243**, 409 (1995).
[105]T. Yanai, D. Tew, and N. Handy, Chem. Phys. Lett. **393**, 51 (2004).
[106]H. Lami, Chem. Phys. Lett. **48**, 447 (1977).
[107]N. A. Borisevich, A. A. Suldiodola, and G. B. Tolstorozhev, Chem. Phys. **354**, 44 (2008).
[108]J. Lipinski and H. Chojnacki, Spectrochim. Acta, Part A **51**, 381 (1995).
[109]H. Lippert, H.-H. Ritze, I. V. Hertel, and W. Radloff, Chem. Phys. Lett. **398**, 526 (2004).
[110]M. Parać and S. Grimme, J. Phys. Chem. A **106**, 6844 (2002).
[111]A. L. Sobolewski and W. Domcke, J. Phys. Chem. A **111**, 11725 (2007).
[112]M. G. D. Nix, A. L. Devine, B. Cronin, and M. N. R. Ashfold, Phys. Chem. Chem. Phys. **8**, 2610 (2006).
[113]A. Iqbal and G. Stavos, J. Phys. Chem. A **114**, 68 (2010).
[114]A. Lange and J. M. Herbert, J. Chem. Theory Comput. **3**, 1680 (2007).
[115]T. Bizjak, Ph.D. dissertation, Ludwig-Maximilians-Universität München, 2004.